IEEE Access
Multidisciplinary | Rapid Review | Open Access Journal

Received 20 June 2023, accepted 6 July 2023, date of publication 11 July 2023, date of current version 26 July 2023.

Digital Object Identifier 10.1109/ACCESS.2023.3293823

RESEARCH ARTICLE

Intelligent Controlled Dynamic Voltage Restorer for Improving Transient Voltage Quality

KUANG-HSIUNG TAN[1], (Member, IEEE), JUN-HAO CHEN[1], AND YIH-DER LEE[2], (Member, IEEE)
[1]Department of Electrical and Electronic Engineering, Chung Cheng Institute of Technology, National Defense University, Taoyuan 335, Taiwan
[2]Nuclear Instrumentation Division, Institute of Nuclear Energy Research, Taoyuan 325, Taiwan

Corresponding author: Kuang-Hsiung Tan (s913115@gmail.com)

This work was supported by the Institute of Nuclear Energy Research of Taiwan under Grant 112A015.

ABSTRACT A dynamic voltage restorer (DVR) is developed to stabilize the three-phase load voltage under the sudden grid voltage distortion conditions, including the voltage sag, swell and unbalance. The DVR is composed of a DC\AC inverter and a DC-link capacitor regarded as the energy storage element. When the sudden grid voltage distortion occurs, the instant power to compensate or absorb is realized by the DC-link capacitor of the DVR resulted in the degenerate stabilization performance and the poor transient voltage quality of the load. Hence, the DC-link voltage control of the DVR for maintaining the constant DC voltage plays an important role in stabilizing the three-phase load voltage. In this study, to improve the transient responses of the three-phase load voltage and the DC-link voltage under the sudden grid voltage distortion conditions, a novel recurrent compensation petri fuzzy neural network (RCPFNN) controller is firstly proposed to replace the conventional proportional-integral (PI) and fuzzy neural network (FNN) controllers for the DC-link voltage control of the DVR. The detailed network structure and the online learning algorithm of the proposed RCPFNN controller are derived. Moreover, some experimental results are given to verify the feasibility and effectiveness of the DVR using the proposed RCPFNN controller for improving the transient voltage quality of the load.

INDEX TERMS Dynamic voltage restorer, voltage quality, voltage sag, intelligent control, recurrent compensation petri fuzzy neural network (RCPFNN).

NOMENCLATURE AND ABBREVIATION

v_{Sa}, v_{Sb}, v_{Sc}	Three-phase grid voltages.
L_s, R_s	Grid impedance.
C_{dc}	DC-link capacitor.
L_{sf}, C_{sf}	LC filter.
T_{sf}	Series transformer.
V_{dc}	DC-link voltage.
v_{Ca}, v_{Cb}, v_{Cc}	Three-phase compensating voltages of DVR.
v_{La}, v_{Lb}, v_{Lc}	Three-phase load voltages.
$v_{S\alpha}, v_{S\beta}$	$\alpha\beta$-axis grid voltages.
$v_{S\alpha}', v_{S\beta}'$	$\alpha\beta$-axis filtered voltages.
$v_{S\alpha}^+, v_{S\beta}^+$	$\alpha\beta$-axis positive-sequence components of grid voltages.
v_{Sd}^+	d-axis positive-sequence voltage.
ω_e	Angular frequency.
θ_e	Electrical angle.
v_{Sd}, v_{Sq}	dq-axis grid voltages.
$\bar{v}_{Sd}, \bar{v}_{Sq}$	dq-axis DC voltage components.
V_m	Actual amplitude of load voltage.
V_m^*	Load voltage command.
v_{Ed}	Reactive component of voltage.
V_{dc}^*	DC-link voltage command.
v_{Eq}	DC-link control voltage.
$v_{La}^*, v_{Lb}^*, v_{Lc}^*$	Three-phase voltage commands.
v_a, v_b, v_c	Three-phase control signals of PWM.
x_i^1	Input variables of RCPFNN.
e	DC-link voltage error.
$\dot{e}$	Derivative of DC-link voltage error.
N	Nth iteration.
y_i^1	Input variable of membership layer.
σ_j^2	Standard deviation of Gaussian function.

The associate editor coordinating the review of this manuscript and approving it for publication was Zhilei Yao.

m_j^2	Mean of Gaussian function.
y_j^2	Output of membership layer.
w_{jk}^3	Connected weight between membership layer and rule layer.
y_k^3	Output of rule layer.
d_{th}	Dynamic threshold value.
t_d^4	Transition of PN.
α, β	Positive parameters of PN.
y_d^4	Output of petri layer.
w_{rc}^5	Recurrent weight.
μ_c^I	Input of recurrent and compensation layer.
y_c^5	Output of recurrent and compensation layer.
γ_1	Compensatory degree.
c_1, d_1	Compensatory degree parameters.
w_c^6	Connected weight between consequent layer and output layer.
y_o^6	Output of RCPFNN.
E	Error function.
δ_o^6	Error term of output layer.
δ_c^5	Error term of recurrent and compensation layer.
δ_d^4	Error term of petri layer.
δ_k^3	Error term of rule layer.
δ_j^2	Error term of membership layer.
η_1	Learning rate of connected weight between recurrent and consequent layer and output layer.
η_2, η_3	Learning rates of compensatory degree parameters.
η_4	Learning rate of recurrent weight.
η_5	Learning rate of mean of Gaussian function.
η_6	Learning rate of standard deviation of Gaussian function.
DVR	Dynamic voltage restorer.
PI	Proportional-integral.
DG	Distributed generator.
PV	Photovoltaic.
FNN	Fuzzy neural network.
CFNN	Compensatory fuzzy neural network.
RNN	Recurrent neural network.
PN	Petri net.
RCPFNN	Recurrent compensation petri fuzzy neural network.
SRF-PLL	Synchronous reference frame phase locked loop.
SOGI-PLL	Second-order generalized integrator phase locked loop.
LP	Low pass.
PWM	Pulse width modulation.
DSP	Digital signal processor.

I. INTRODUCTION

Nowadays, in consequence of the global warming, greenhouse gas emission problem and energy crisis, the penetration rate of the renewable energy-based distributed generator (DG) such as wind turbine generator and photovoltaic (PV) system has been increasing in the utility grid [1], [2], [3], [4]. Moreover, with the increasing critical and sensitive loads, including the adjustable speed drives, computing equipment, switched mode power supplies, communication system, and so on, the power quality issue has been gotten noteworthy attention [5], [6]. However, owing to the high intermittency of the renewable energy resources, unexpected load changes, short circuits and direct-off-line power electronic system, the power quality will be reduced to cause the overload, failure and equipment downtime leading to lost revenue [7], [8]. In other words, the voltage distortion problems, including the grid voltage sag, swell and unbalance, arise and seriously affect the sensitive loads in the power system [9], [10]. According to IEEE 1159-2019 standard [11], the grid voltage sag is defined that the temporary drop of the RMS voltage decreases from 0.1 per unit (pu) to 0.9 pu over a time longer than 0.5 cycles of system frequency but less than 60 seconds. On the other hand, the grid voltage swell is indicated that the RMS voltage is temporarily increased and the start threshold is 1.1 pu [11], [12]. Hence, it is an important issue for the utility grid to stabilize the three-phase load voltage under the sudden grid voltage sag, swell and unbalance conditions.

The dynamic voltage restorer (DVR) is one of the widespread solutions to mitigate the abnormal grid voltage. The main function of the DVR is to instantly inject a voltage compensation with the exact phase and magnitude in series with the source grid. Thus, the three-phase load voltage can be maintained the constant and normal voltage level under the grid voltage sag, swell and unbalance conditions [13], [14], [15]. In terms of the structure, the DVR can be classified into two categories: 1) DVR without energy storage; 2) DVR with energy storage such as the flywheel, capacitor and battery [16]. The power energy for the voltage compensation or absorption of the DVR without energy storage is achieved by the faulted source grid. Hence, the DVR without energy storage can compensate or absorb for longer sag, swell and unbalance. However, the main demerit is the use of the AC\DC converter to connect with the faulted source grid. Consequently, the power losses and cost of the DVR without energy storage will be increased [17]. And the DVR without energy storage may be broken down due to the connection with faulted source grid. On the other hand, the DVR with energy storage isn't equipped with the AC\DC converter to connect with the source grid. The power energy for the voltage compensation or absorption of the DVR with energy storage is realized by the DC-link capacitor or battery. Thus, owing to the simple structure, the DVR with energy storage is a cost-effective solution [18]. Some researches using the DVR for improving the voltage distortion have been proposed [19], [20], [21], [22]. A hybrid energy storage system using robust control algorithm was proposed in [19] to provide superior power supply for multilevel inverter part of the DVR. In [20], an innovative AC voltage synthesizer based on two novelties for the

DVR to compensate the voltage disturbances and ride-through the faults during the voltage disturbance conditions. A photovoltaic system with half-cascaded multilevel inverter is proposed for the DVR to improve the power quality [21]. In [22], two PI-particle swarm optimization controllers were provided to stimulate a DVR for enhancing the on-grid hybrid system under misfire and fire-through faults. In general, the DVR with the DC-link capacitor is widely adopted. However, when the sudden grid voltage distortion conditions occur, the instant power follows into or out of the DC-link capacitor of the DVR resulted in the degenerate stabilization performance and the poor transient voltage quality of the load [18]. Hence, the DC-link voltage control of the DVR for maintaining the constant DC-link voltage plays an important role in stabilizing the three-phase load voltage under the sudden grid voltage sag, swell and unbalance conditions. However, the sluggish regulation of the DC-link voltage of the DVR was obtained by the traditional PI controller in the literature [9], [10], [12], [16].

Though the traditional fuzzy neural network (FNN) has been widely adopted in industrial applications, the fixed fuzzy operator cannot optimize the fuzzy logic reasoning. Moreover, there are not enough free variables to modify the fuzzy operator [23]. Consequently, the compensatory fuzzy neural network (CFNN) has been proposed to solve the demerits of the conventional FNN. The CFNN integrates the compensatory operation with the FNN to adaptively adjust fuzzy membership function and dynamically optimize the adaptive fuzzy operation [24], [25]. Furthermore, the pessimistic fuzzy neuron, optimistic fuzzy neuron, and compensatory fuzzy neuron are implemented by the CFNN to make a superior decision for the situation between the worst and the best cases [26]. Thus, the CFNN is superior to the traditional FNN. The researches using the CFNN for different applications have been proposed [25], [26]. In [25], a photovoltaic system using CFNN controller is proposed to compensate the three-phase unbalanced grid currents under the unbalanced loads. A CFNN with an asymmetric membership function controller is investigated for the distribution static compensator to improve the power quality [26]. Lately, the recurrent neural network (RNN) is developed by using the feedback connections to memorize the temporal characteristics of the input data set [27]. Hence, the RNN is more powerful than the traditional feedforward networks [28]. In other words, since the recurrent connections of the RNN endow the network with memory to obtain more system information, the RNN possesses the ability to deal with the time-varying inputs or outputs and the capability to process the complicated spatiotemporal patterns [29]. In addition, petri net (PN) is a mathematical and graphical tool and is suitable for deadlock analysis, scheduling and control in the automated manufacturing system [30], [31]. Accordingly, the PN possesses the abilities in analysis, modeling and simulation, and the capability to control the various discrete event systems [32]. Hence, in accordance with the merits of the CFNN, RNN and PN, a novel recurrent compensation petri fuzzy neural network (RCPFNN) controller is firstly proposed in this study.

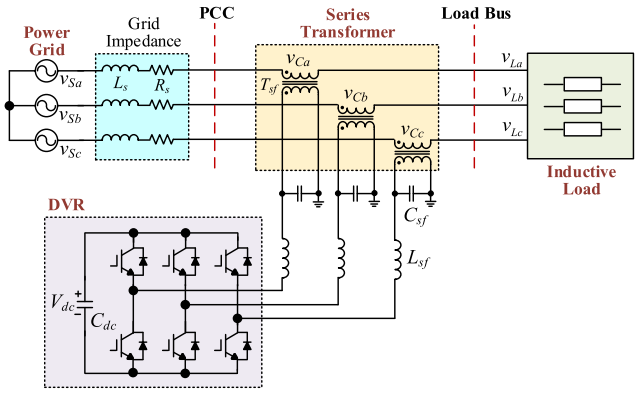

FIGURE 1. Configuration of DVR connected in series with power grid and load.

In this study, a DVR with the DC-link capacitor is developed to stabilize the three-phase load voltage. To improve the transient responses of the three-phase load voltage and the DC-link voltage of the DVR under the sudden grid voltage distortion conditions, including the voltage sag, swell and unbalance, a novel RCPFNN controller is firstly proposed as the DC-link voltage controller to replace the conventional PI and FNN controllers for maintaining the constant DC-link voltage of the DVR. The main contributions of this study are aggregated in the following:

- The successful development of a DVR.
- The successful development of a novel online trained RCPFNN controller for the compensation strategy and the DC-link voltage control of the DVR.
- The successful implementation of the DVR using the proposed RCPFNN controller for the improvements of the three-phase load voltage and DC-link voltage under the sudden grid voltage distortion conditions, including the voltage sag, swell and unbalance.

The operation theories of the DVR will be described in Section II. The detailed network structure and online learning algorithm of the proposed RCPFNN controller are derived in Section III. Then, the feasibility and effectiveness of the DVR using the proposed RCPFNN controller for stabilizing the three-phase load voltage and the DC-link voltage under the sudden grid voltage sag, swell and unbalance conditions are verified by the experimental results compared with the PI and FNN controlled DVRs in Section IV. Finally, some conclusions are provided in Section V.

II. OPERATION THEORIES OF DVR

The configuration of the DVR with the DC-link capacitor C_{dc} is given in Fig. 1. The DVR is connected to the primary winding of the series transformer with the turn ratio 1 through the LC filter (L_{sf}, C_{sf}) and connected in series with the power grid before the inductive load via the secondary winding of the transformer [15], [16]. In this study, the line to line voltage

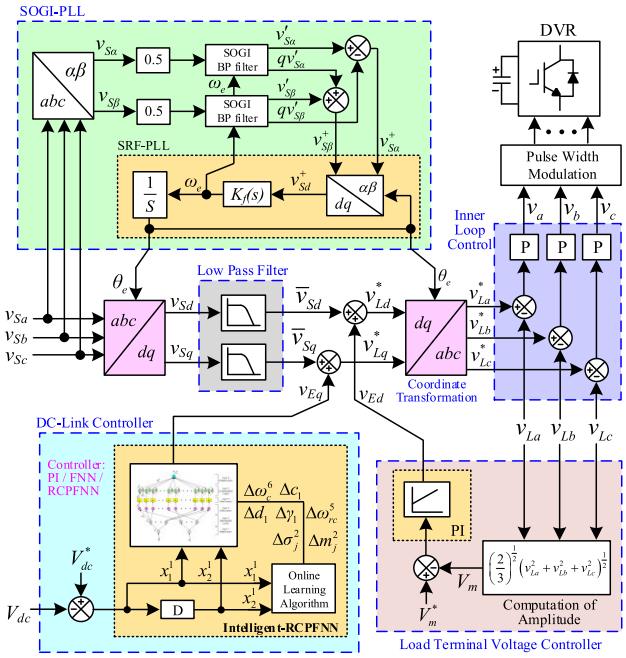

FIGURE 2. Block diagram of DVR using proposed RCPFNN controller for compensation strategy and DC-link voltage control.

and frequency of the power grid are 220 Vrms and 60 Hz, respectively.

A. SYNCHRONIZATION ALGORITHM

The block diagram of the DVR using the proposed RCPFNN controller for the compensation strategy and DC-link voltage control is illustrated in Fig. 2. In order to effectively synchronize with the power grid, a dual second-order generalized integrator phase locked loop (SOGI-PLL) is adopted for the grid synchronization. The dual SOGI-PLL is developed based on the traditional synchronous reference frame PLL (SRF-PLL). The purpose of the dual SOGI-PLL is to overcome the demerit of the SRF-PLL such as the inaccuracy in faulty grid [33]. The SOGI-PLL can obtain the accurate electric angle θ_e by using the positive-sequence components of the grid voltages during the distorted conditions [33]. According to the algorithm of the SOGI-PLL, the three-phase grid voltages v_{Sa}, v_{Sb}, v_{Sc} are detected and the $\alpha\beta$ -axis voltages $v_{S\alpha}, v_{S\beta}$ are calculated by using the $abc/\alpha\beta$ coordinate transformation as follows:

$$\begin{bmatrix} v_{S\alpha} \\ v_{S\beta} \end{bmatrix} = \frac{2}{3}\begin{bmatrix} 1 & -\frac{1}{2} & -\frac{1}{2} \\ 0 & -\frac{\sqrt{3}}{2} & -\frac{\sqrt{3}}{2} \end{bmatrix}\begin{bmatrix} v_{Sa} \\ v_{Sb} \\ v_{Sc} \end{bmatrix} \tag{1}$$

The filtered voltages $v_{S\alpha}^{'}, v_{S\beta}^{'}$ are extracted by using the $\alpha\beta$ axis voltages $v_{S\alpha}, v_{S\beta}$ through the band-pass (BP) filters. Then, the positive-sequence components of the grid voltages $v_{S\alpha}^{+}, v_{S\beta}^{+}$ are obtained as follows:

$$\begin{bmatrix} v_{S\alpha}^{+} \\ v_{S\beta}^{+} \end{bmatrix} = \frac{1}{2}\begin{bmatrix} 1 & -q \\ q & 1 \end{bmatrix}\begin{bmatrix} v_{S\alpha}^{'} \\ v_{S\beta}^{'} \end{bmatrix}, q = e^{j\frac{\pi}{2}} \tag{2}$$

where q is a phase-shift operator in the time domain. The positive-sequence components $v_{S\alpha}^{+}$, $v_{S\beta}^{+}$ are sent to the traditional SRF-PLL and transformed to the dq-axis positive-sequence components via the $\alpha\beta/dq$ coordinate transformation. The d-axis positive-sequence voltage v_{Sd}^{+} is computed as:

$$v_{Sd}^{+} = v_{S\alpha}^{+}\cos\theta_e - v_{S\beta}^{+}\sin\theta_e \tag{3}$$

The angular frequency ω_e is calculated by using the d-axis positive-sequence voltage v_{Sd}^{+} via a proportional controller $K_f(s)$. Then, the electric angle θ_e can be obtained for grid synchronization by using the integral operation.

B. CONTROL ALGORITHM OF DVR

In Fig. 2, the three-phase grid voltages v_{Sa}, v_{Sb}, v_{Sc} are transformed to the dq-axis grid voltages v_{Sd}, v_{Sq} by using the $abc/\alpha\beta$ coordinate transformation. The dq -axis grid voltages v_{Sd}, v_{Sq} consist of the DC component and oscillatory component [10]. The dq-axis DC voltage components $\bar{v}_{Sd}$, $\bar{v}_{Sq}$ are extracted by the low pass (LP) filters. Then, the three-phase load voltages v_{La}, v_{Lb}, v_{Lc} are detected to obtain the actual amplitude V_m of the load voltage by using the following equation:

$$V_m = \sqrt{\frac{2}{3}(v_{La}^2 + v_{Lb}^2 + v_{Lc}^2)} \tag{4}$$

The difference between the load voltage command V_m^* and the actual amplitude V_m of the load voltage is sent to the PI controller to generate the reactive component of voltage v_{Ed} for the regulation of the voltage at the load terminal [10]. The d-axis voltage command$v_{Ld}^*$is acquired by adding the reactive component of voltage v_{Ed} to the d-axis DC voltage component $\bar{v}_{Sd}$. Moreover, in this study, to effectively maintain the constant DC-link voltage of the DVR under the sudden grid voltage sag, swell and unbalance, the DC-link voltage command V_{dc}^* is compared with the actual DC-link voltage V_{dc} to acquire the DC-link voltage error $V_{dc}^* - V_{dc}$. Then, the DC-link voltage error is sent to the traditional PI, FNN or the proposed RCPFNN controller to generate the voltage component v_{Eq} for compensating the power loss and the DC-link voltage control. Thereupon, the voltage component v_{Eq} is added to the q-axis DC voltage component $\bar{v}_{Sq}$ to generate the q-axis voltage command v_{Lq}^*. Then, the three-phase voltage commands $v_{La}^*, v_{Lb}^*, v_{Lc}^*$ are computed by using the dq/abc coordinate transformation as follows to generate the control signals v_a, v_b, v_c via P controllers for the generation of the pulse width modulation (PWM) switching signals of the DVR with the DC-link capacitor.

$$\begin{bmatrix} v_{La}^* \\ v_{Lb}^* \\ v_{Lc}^* \end{bmatrix} = \begin{bmatrix} 1 & 0 \\ -\frac{1}{2} & -\frac{\sqrt{3}}{2} \\ -\frac{1}{2} & \frac{\sqrt{3}}{2} \end{bmatrix}\begin{bmatrix} \cos\theta_e & -sin\theta_e \\ \sin\theta_e & \cos\theta_e \end{bmatrix}\begin{bmatrix} v_{Ld}^* \\ v_{Lq}^* \end{bmatrix} \tag{5}$$

Consequently, according to the above compensation strategy of the DVR, since the q-axis voltage command v_{Lq}^* is composed of the voltage component v_{Eq} generated by the DC-link voltage error $V_{dc}^* - V_{dc}$ through the proposed RCPFNN

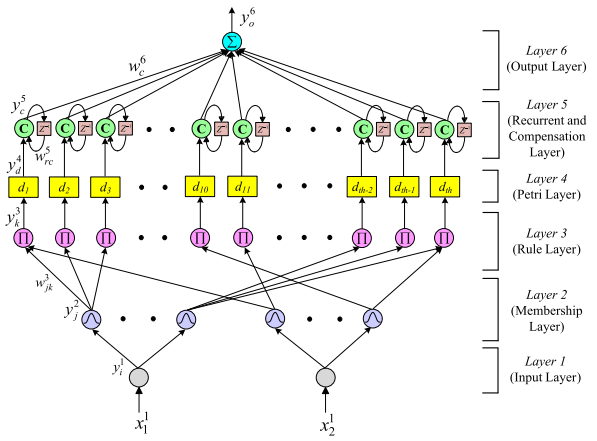

FIGURE 3. Network structure of proposed RCPFNN controller.

controller for compensating the power loss and the DC-link voltage control, the proposed RCPFNN controller for the DVR can improve the three-phase load voltages and DC-link voltage under the grid voltage distortion conditions.

III. INTELLIGENT RCPFNN CONTROLLER

Though the PI controller is popularly employed in different applications on account of its simple structure and easy implementation, some disadvantages of the PI controller, including the poor disturbance rejection, degenerate the control performance [3], [4]. Moreover, since the fixed parameters of the PI controller are designed only for the hypothetical scenarios, the performance of the PI controller will be decreased in the case of the external disturbance and interference such as the sudden grid voltage sag, swell and unbalance. On the other hand, owing to the power following into or out of the DC-link capacitor of the DVR resulted in the degenerate stabilization performance and the poor transient responses under the sudden grid voltage distortion conditions, a novel RCPFNN controller is firstly proposed as the DC-link voltage controller to replace the traditional PI and FNN controllers for improving the transient responses of the three-phase load voltage and the DC-link voltage of the DVR under the sudden grid voltage distortion conditions. The proposed six-layer RCPFNN controller comprises the input layer, membership layer, rule layer, petri layer, recurrent and compensation layer, and the output layer. Furthermore, the network structure of the proposed RCPFNN controller is represented in Fig. 3. The network structure and online learning algorithm of the six-layer RCPFNN controller are detailedly derived as follows:

A. NETWORK STRUCTURE

1) INPUT LAYER

The relationship between the inputs and the outputs of the node in this layer is given as:

$$net_i^1(N) = x_i^1 \tag{6}$$

$$y_i^1(N) = f_i^1\left(net_i^1(N)\right) = net_i^1(N), i = 1, 2 \tag{7}$$

The input variables of the proposed RCPFNN are $x_1^1 = e(t) = V_{dc}^* - V_{dc}$ for the DC-link voltage control of the DVR, and its derivative $x_2^1 = \dot{e}(t)$. N expresses the Nth iteration.

2) MEMBERSHIP LAYER

In membership layer, the fuzzification operation is carried out by each node employing a Gaussian function. The signal propagation of this layer is described in the following:

$$net_j^2(N) = -\frac{\left(y_i^1(N) - m_j^2(N)\right)^2}{\left(\sigma_j^2(N)\right)^2}; i = 1, 2; j = 1, \ldots, h \tag{8}$$

$$y_j^2(N) = f_j^2\left(net_j^1(N)\right) = \exp(net_j^2(N)) \tag{9}$$

where $h = 6$ represents the total number of the linguistic variables. σ_j^2 and m_j^2 denote the standard deviation and the mean of the Gaussian function, respectively.

3) RULE LAYER

In this layer, the multiplication operation denoted by $\prod$ is implemented to multiply the input signals and output the result of product.

$$net_k^3(N) = \prod_j w_{jk}^3 y_j^2(N) \tag{10}$$

$$y_k^3(N) = f_k^3\left(net_k^3(N)\right) = net_k^3(N); \quad k = 1, 2, \ldots, m \tag{11}$$

where $m = 25$ is the total number of the linguistic variables. $w_{jk}^3 = 1$ is the connected weight between the membership layer and the rule layer.

4) PETRI LAYER

In accordance with the PN theory, the competition law is utilized to select the suitable fired nodes for generating the tokens in the petri layer [3], [4]. The PN is composed of two types of nodes: transition and place. When the token is created in input place, the transition is in enable state. Consequently, the condition of the fired or unfired transition can be described as:

$$t_d^4 = \begin{cases} 1, y_k^3 > d_{th} \\ 0, y_k^3 < d_{th}, \end{cases} \quad th = 1, 2, \ldots, m \tag{12}$$

$$d_{th} = \frac{\alpha \exp(-\beta V)}{1 + \exp(-\beta V)} \tag{13}$$

where $t_d^4(N)$ is the transition; α and β are positive constants. The dynamic threshold value d_{th} is varied by the function Vin the following [3]:

$$V = \frac{1}{2}(x_1^1(N) + x_2^1(N)) \tag{14}$$

When the transitions are fired, the required tokens are removed from its input places and new tokens are generated at each output place. On the other hand, when the transitions are

unfired, the token will stay in original input place. Thereupon, the output and input of this layer are given as:

$$net_d^4(N) = \begin{cases} y_k^3(N), t_d^4(N) = 1 \\ 0, t_d^4(N) = 0 \end{cases} \tag{15}$$

$$y_d^4(N) = f_d^4\left(net_d^4(N)\right) = net_d^4(N), \quad d = 1, 2, \ldots, m \tag{16}$$

5) RECURRENT AND COMPENSATION LAYER

The precondition part of the fuzzy logic rules is realized by the nodes in this layer. The compensatory parameters are integrated with this layer to execute IF-condition matching of fuzzy rules. Consequently, the relationship between the input and output of the recurrent and compensation layer is derived in the following:

$$\mu_c^I = \prod_c [y_d^4(N) w_{rc}^5 y_c^5(N-1)] \tag{17}$$

$$net_c^5(N) = (\mu_c^I)^{1-\gamma_l+\frac{\gamma_l}{n}}, \quad \gamma_l = [0, 1], n = 2 \tag{18}$$

$$y_c^5(N) = f_c^5\left(net_c^5(N)\right) = net_c^5(N), \quad c = 1, 2, \ldots, m \tag{19}$$

where $\mu_c^I(N)$ and $y_c^5(N)$ are the input and output of this layer, respectively; w_{rc}^5 is the recurrent weight to memorize the temporal characteristics of the input signals; γ_1 expresses the compensatory degree. If γ_l is trained online, the compensatory operation becomes more adaptive. Moreover, in order to guarantee $\gamma_l \in [0, 1]$, the compensatory degree γ_l is defined as [24], [25]:

$$\gamma_1 = \frac{c_l^2}{c_l^2 + d_l^2} \tag{20}$$

where parameters c_l and d_l will be trained real-time.

6) OUTPUT LAYER

The defuzzification is performed by using the summation operation Σ and depicted as follows:

$$net_o^6(N) = \sum_l w_c^6 y_c^5(N) \tag{21}$$

$$y_o^6(N) = f_o^6(net_0^6(N)) = net_0^6(N), \quad o = 1 \tag{22}$$

where w_c^6 is the connected weight between the output layer and the recurrent and compensation layer; $y_o^6(N)$ is the output of the proposed RCPFNN and is also equal to the voltage component v_{Eq} as shown in Fig. 2 for the DC-link voltage control of the DVR.

B. ONLINE LEARNING

In the proposed RCPFNN, the online learning using a supervised gradient decent method to minimize a given error function E is utilized in this study. The principle of the online learning algorithm is to online tune the parameters of the proposed RCPFNN. In this study, the error function E is given in the following [3]:

$$E = \frac{1}{2}(V_{dc}^* - V_{dc})^2 = \frac{1}{2}e^2 \tag{23}$$

Thereupon, the procedure of the learning algorithm of proposed RCPFNN is detailedly derived as follows:

1) OUTPUT LAYER

In this layer, the error term to be propagated is derived as:

$$\delta_o^6 = -\frac{\partial E}{\partial y_o^6(N)} = -\frac{\partial E}{\partial V_{dc}} \frac{\partial V_{dc}}{\partial y_o^6(N)} \tag{24}$$

In accordance with the chain rule, the connected weight is computed and updated by the following amount.

$$\Delta w_c^6 = -\eta_1 \frac{\partial E}{\partial w_c^6(N)} = -\eta_1 \frac{\partial E}{\partial y_o^6(N)} \frac{\partial y_o^6(N)}{\partial w_c^6(N)} = \eta_1 \delta_o^6 y_c^5 \tag{25}$$

where η_1 is the learning rate. Then, the connected weight w_c^6 is updated as:

$$w_c^6(N+1) = w_c^6(N) + \Delta w_c^6 \tag{26}$$

2) RECURRENT AND COMPENSATION LAYER

The error term to be propagated and computed is described in the following:

$$\delta_c^5 = -\frac{\partial E}{\partial y_c^5(N)} = -\frac{\partial E}{\partial y_o^6} \frac{\partial y_o^6}{\partial y_c^5(N)} = \delta_o^6 w_c^6 \tag{27}$$

Since the compensatory degree γ_l is composed of the parameters c_l and d_l, the updates of the compensatory degree γ_l and the parameters c_l and d_l are calculated by the following amounts:

$$\begin{aligned} \Delta c_l &= -\eta_2 \frac{\partial E}{\partial c_l(N)} = -\eta_2 \frac{\partial E}{\partial \gamma_l(N)} \frac{\partial \gamma_l(N)}{\partial c_l(N)} \\ &= -\eta_2 \frac{\partial E}{\partial \gamma_l(N)} \frac{2c_l(N) d_l(N)^2}{\left(c_l(N)^2 + d_l(N)^2\right)^2} \\ &= \eta_2 \Delta\gamma_l \frac{2c_l(N) d_l(N)^2}{\left(c_l(N)^2 + d_l(N)^2\right)^2} \end{aligned} \tag{28}$$

$$\begin{aligned} \Delta d_l &= -\eta_3 \frac{\partial E}{\partial d_l(N)} = -\eta_3 \frac{\partial E}{\partial \gamma_l(N)} \frac{\partial \gamma_l(N)}{\partial d_l(N)} \\ &= -\eta_3 \frac{\partial E}{\partial \gamma_l(N)} \frac{-2c_l(N)^2 d_l(N)}{\left(c_l(N)^2 + d_l(N)^2\right)^2} \\ &= \eta_3 \Delta\gamma_l \frac{-2c_l(N)^2 d_l(N)}{\left(c_l(N)^2 + d_l(N)^2\right)^2} \end{aligned} \tag{29}$$

$$\begin{aligned} \Delta\gamma_l &= \frac{\partial E}{\partial \gamma_l(N)} = -\frac{\partial E}{\partial y_c^5(N)} \frac{\partial y_c^5(N)}{\partial \gamma_l(N)} \\ &= \delta_c^5 \left(\frac{1}{n} - 1\right) \left(\mu_c^I\right)^{1-\gamma_l+\frac{\gamma_l}{n}} \ln(\mu_c^I)^{1-\gamma_l+\frac{\gamma_l}{n}} \end{aligned} \tag{30}$$

$$\begin{aligned} \Delta w_{rc}^5 &= -\eta_4 \frac{\partial E}{\partial w_{rc}^5(N)} = -\eta_4 \frac{\partial E}{\partial y_o^6(N)} \frac{\partial y_o^6(N)}{\partial y_c^5(N)} \frac{\partial y_c^5(N)}{\partial w_{rc}^5(N)} \\ &= \eta_4 \delta_c^5 (1 - \gamma_l + \frac{\gamma_l}{n}) \left(\mu_c^I\right)^{-\gamma_l+\frac{\gamma_l}{n}} \prod_c [y_d^4(N) y_c^5(N-1)] \end{aligned} \tag{31}$$

where η_2, η_3 and η_4 are the learning rates. The updated values of the parameters c_l and d_l, the compensatory degree γ_l, and the recurrent weight w_{rc}^5 are acquired as:

$$\begin{aligned} c_l(N+1) &= c_l(N) + \Delta c_l \\ &= c_l(N) + \eta_2 \left\{ \frac{2c_l(N)\, d_l^2(N)}{\left[c_l^2(N) + d_l^2(N)\right]^2} \right\} \Delta\gamma_l \end{aligned} \tag{32}$$

$$\begin{aligned} d_l(N+1) &= d_l(N) + \Delta d_l \\ &= d_l(N) + \eta_3 \left\{ \frac{2c_l^2(N)\, d_l(N)}{\left[c_l^2(N) + d_l^2(N)\right]^2} \right\} \Delta\gamma_l \end{aligned} \tag{33}$$

$$\gamma_l(N+1) = \frac{c_l^2(N+1)}{c_l^2(N+1) + d_l^2(N+1)} \tag{34}$$

$$w_{rc}^5(N+1) = w_{rc}^5(N) + \Delta w_{rc}^5 \tag{35}$$

3) PETRI LAYER

The error term of the petri layer is obtained as follows:

$$\begin{aligned} \delta_d^4 &= -\frac{\partial E}{\partial y_d^4(N)} = -\frac{\partial E}{\partial y_c^5(N)} \frac{\partial y_c^5(N)}{\partial y_d^4(N)} \\ &= \delta_c^5 (1 - \gamma_l + \frac{\gamma_l}{n}) \left(\mu_c^l\right)^{-\gamma_l + \frac{\gamma_l}{n}} \prod_c \left[w_{rc}^5 y_c^5(N-1)\right] \end{aligned} \tag{36}$$

4) RULE LAYER

In rule layer, the term of the propagated error can be derived as:

$$\delta_k^3 = -\frac{\partial E}{\partial y_k^3(N)} = -\frac{\partial E}{\partial y_d^4(N)} \frac{\partial y_d^4(N)}{\partial y_k^3(N)} = \delta_d^4 t_d^4 \tag{37}$$

5) MEMBERSHIP LAYER

In this layer, the propagated error term is depicted as:

$$\begin{aligned} \delta_j^2 &= -\frac{\partial E}{\partial net_j^2(N)} \\ &= -\frac{\partial E}{\partial y_k^3(N)} \frac{\partial y_k^3(N)}{\partial y_j^2(N)} \frac{\partial y_{j(N)}^2}{\partial net_j^2(N)} = \sum_k \delta_k^3 y_k^3 \end{aligned} \tag{38}$$

Hence, the updates of the mean Δm_j^2 and standard deviation $\Delta\sigma_j^2$ of the membership functions are represented in the following:

$$\begin{aligned} \Delta m_j^2 &= -\eta_5 \frac{\partial E}{\partial m_j^2(N)} \\ &= -\eta_5 \frac{\partial E}{\partial y_k^3(N)} \frac{\partial y_k^3(N)}{\partial y_j^2(N)} \frac{\partial y_j^2(N)}{\partial net_j^2(N)} \frac{\partial net_j^2(N)}{\partial m_j^2(N)} \\ &= \eta_5 \delta_j^2 \frac{2(y_i^1 - m_j^2)}{(\sigma_j^2)^2} \end{aligned} \tag{39}$$

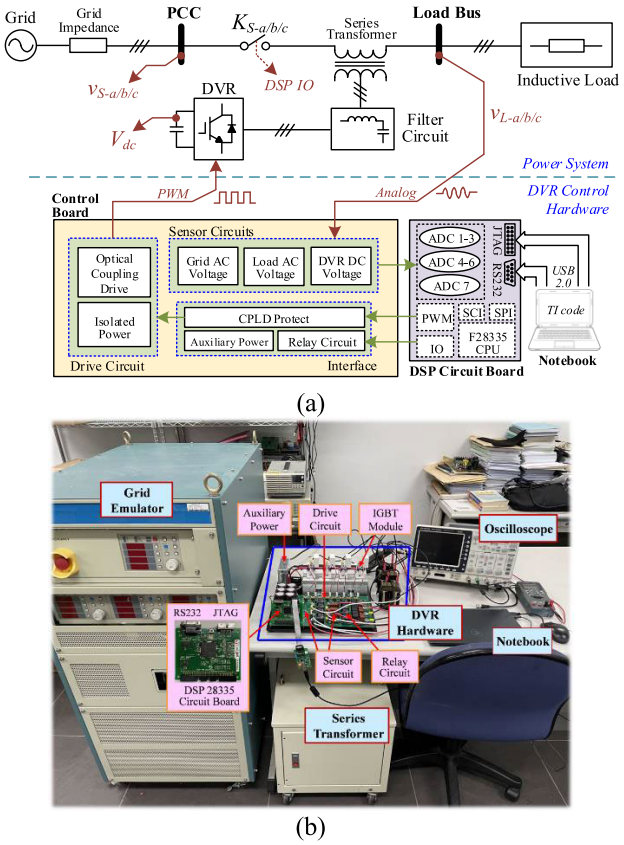

FIGURE 4. Designed DVR control platform. (a) Block diagram of DSP-based DVR. (b) Photo of experimental setup.

$$\begin{aligned} \Delta\sigma_j^2 &= -\eta_6 \frac{\partial E}{\partial \sigma_j^2(N)} \\ &= -\eta_6 \frac{\partial E}{\partial y_k^3(N)} \frac{\partial y_k^3(N)}{\partial y_j^2(N)} \frac{\partial y_j^2(N)}{\partial net_j^2(N)} \frac{\partial net_j^2(N)}{\partial \sigma_j^2(N)} \\ &= \eta_6 \delta_j^2 \frac{2(y_i^1 - m_j^2)^2}{(\sigma_j^2)^2} \end{aligned} \tag{40}$$

where η_5 and η_6 are the learning rates of the mean and standard deviation respectively. Consequently, the updated mean m_j^2 and standard deviation σ_j^2 of the membership functions are given in the following:

$$m_j^2(N+1) = m_j^2(N) + \Delta m_j^2 \tag{41}$$

$$\sigma_j^2(N+1) = \sigma_j^2(N) + \Delta\sigma_j^2 \tag{42}$$

Because of the uncertainties such as external interference, disturbance and parameter variations in the dynamic DVR, the exact calculation of the Jacobian of the DVR, $\partial V_{dc}/\partial y_o^6(N)$, cannot be achieved. Hence, the delta adaptation law is employed to overcome the above problem and to improve the online learning rate of the parameters in the proposed RCPFNN [3], [4].

$$\delta_o^6 \cong e + \dot{e} \tag{43}$$

TABLE 1. Specification of Designed DVR Connected in Series with Power Grid and Load.

Parameters	Values
Grid Voltage : v_S	220 Vrms(L-L), 60 Hz
Grid Impedance : R_s, L_s	1.5m Ω, 0.15 μH
DC-Link Voltage : V_{dc}	450 V
DC-Link Capacitor : C_{dc}	2820 uF
Interfacing Inductor : L_{sf}	3 mH
Ripple Filter : C_{sf}	10 uF
Switching Frequency : f_{sw}	18 kHz
Sampling Frequency : f_s	10 kHz
Series Transformer : T_{sf}	1:1 ratio, 5 kVA
Inductive Load : R_L, L_L	20 Ω, 30 mH

IV. EXPERIMENTAL RESULTS

The DVR to stabilize the three-phase load voltage is developed and provided in Fig. 4. The block diagram of the digital signal processor (DSP)-based DVR is given in Fig. 4(a). The control algorithms of the DVR, including the dual SOGI-PLL and the proposed RCPFNN for the DC-link voltage control are carried out by the DSP TMS320F28335. The control board of the DVR comprises the drive, sensor and the interface circuits. Moreover, the photo of the experimental setup is provided in Fig. 4(b). In this study, an IDRC programmable AC power supply CIF-1530EP9P is adopted to emulate the three-phase faulted grid such as the sudden grid voltage sag, swell and unbalance conditions. Furthermore, the detailed specification of the designed DVR connected in series with the power grid and load is provided in Table 1. Furthermore, the parameters of the PI controller for the DC-link voltage control of the DVR are obtained by trial and error to achieve the best transient and steady-state responses of the DC-link voltage. The proportional gain is 1.3 and the integral gain is 0.38. The proportional gain of the inner loop control is 2.7. The DC-link voltage command V_{dc}^* of the DVR is set to be 450 V. In this study, since the line to line voltage of the power grid is 220 Vrms, the amplitude command V_m^* of the phase voltage is set to be 179 V as shown in Fig. 2. On account of the transient deterioration in the three-phase load voltage and the DC-link voltage of the DVR under the sudden grid voltage distortion conditions, the novel RCPFNN controller is proposed for the DC-link voltage control to improve the transient responses of the load voltage and the DC-link voltage of the DVR in this study. Thus, to verify the effectiveness of the DVR using the proposed RCPFNN for the DC-link voltage control, three test cases are designed in the following: (1) sudden grid voltage sag of 40 % normal value, (2) sudden grid voltage swell of 30 % normal value, and (3) sudden grid voltage unbalance. In addition, the experimental results of the DVR using the PI and FNN controllers are also provided for the comparison.

Firstly, the performance of the DVR under the sudden grid voltage sag is demonstrated. At this scenario, the amplitudes of the three-phase grid voltages decrease from its normal value by 40 % at 0.4 s. The experimental result of the DVR

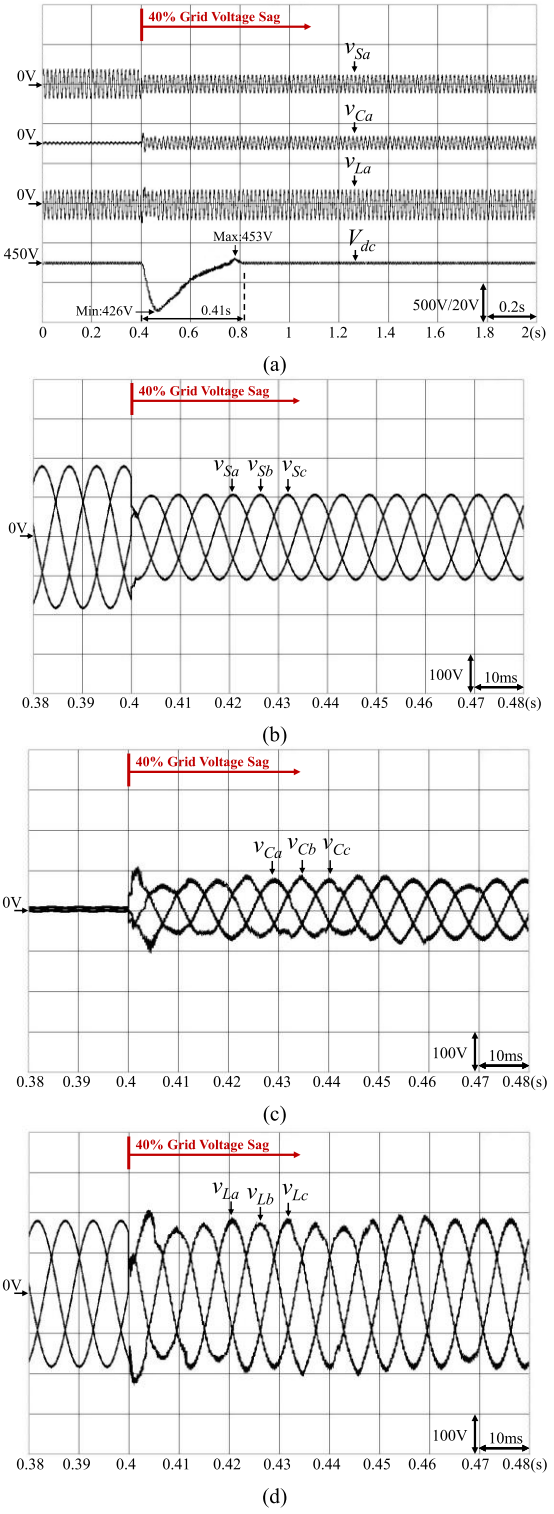

FIGURE 5. Experimental results of DVR using PI controller under voltage sag. (a) Responses of grid voltage, compensating voltage of DVR, load voltage and DC-link voltage of DVR. (b) Responses of three-phase grid voltages for 0.38-0.48 s. (c) Responses of three-phase compensating voltages of DVR for 0.38-0.48 s. (d) Responses of three-phase load voltages for 0.38-0.48 s.

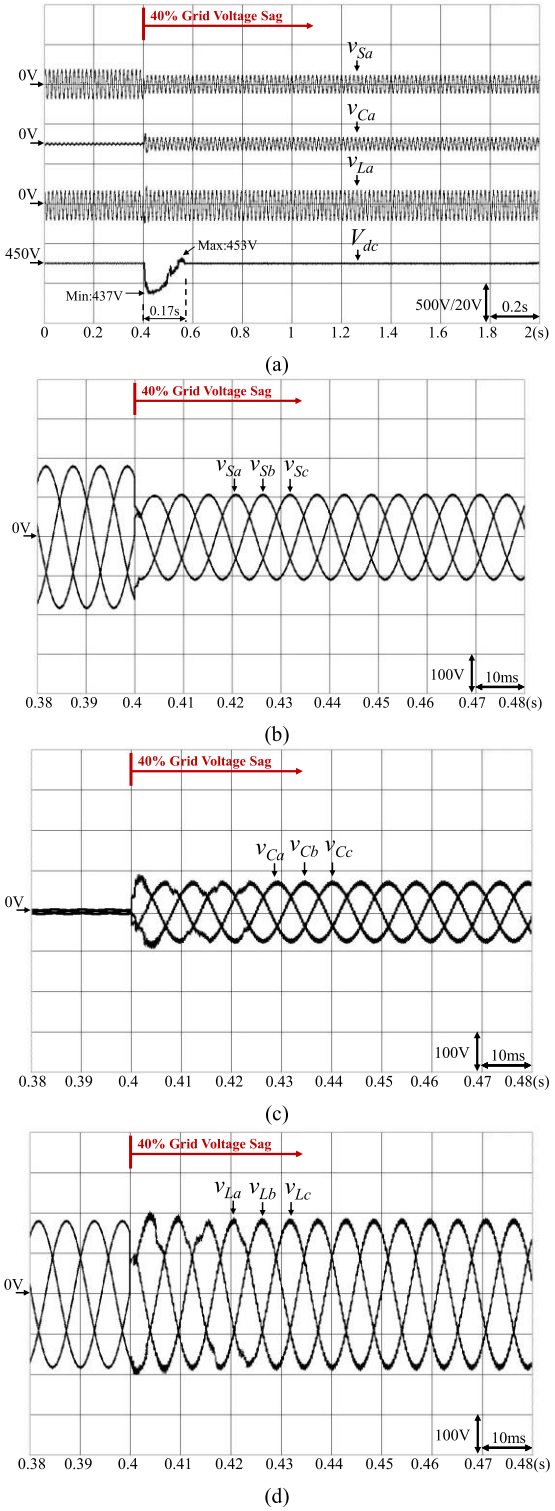

FIGURE 6. Experimental results of DVR using FNN controller under voltage sag. (a) Responses of grid voltage, compensating voltage of DVR, load voltage and DC-link voltage of DVR. (b) Responses of three-phase grid voltages for 0.38-0.48 s. (c) Responses of three-phase compensating voltages of DVR for 0.38-0.48 s. (d) Responses of three-phase load voltages for 0.38-0.48 s.

using PI controller for the DC-link voltage control is provided in Fig. 5. The responses of the grid voltage v_{Sa}, compensating voltage v_{Ca} of the DVR, load voltage v_{La} and the DC-link voltage V_{dc} of the DVR are represented in Fig. 5(a). The responses of the three-phase grid voltages v_{Sa}, v_{Sb}, v_{Sc} in the interval 0.38-0.48 s are provided in Fig. 5(b). The responses of the three-phase compensating voltages v_{Ca}, v_{Cb}, v_{Cc} of the DVR in the interval 0.38-0.48 s are shown in Fig. 5(c). The responses of the three-phase load voltages v_{La}, v_{Lb}, v_{Lc} in the interval 0.38-0.48 s are illustrated in Fig. 5(d). In accordance with the experimental results as shown in Fig. 5, when the power grid is in the normal operation before 0.4 s, the DVR doesn't deliver the compensating voltages v_{Ca}, v_{Cb}, v_{Cc} and the load voltages are equal to the grid voltages v_{Sa}, v_{Sb}, v_{Sc} as shown in Figs. 5(b), 5(c) and 5(d). However, when a sudden voltage sag of 40% normal value occurs at 0.4 s, the DVR dispatches the three-phase compensating voltages v_{Ca}, v_{Cb}, v_{Cc} to maintain the three-phase load voltages v_{La}, v_{Lb}, v_{Lc} as shown in Figs. 5(b), 5(c) and 5(d). Though the effectiveness of the DVR to stabilize the three-phase load voltages is verified, the transient deteriorations in the DC-link voltage V_{dc} of the DVR and the three-phase load voltages v_{La}, v_{Lb}, v_{Lc} are very serious at 0.4 s as shown in Figs. 5(a) and 5(d) due to the disadvantage of the traditional PI controller such as the poor disturbance rejection. The maximum and the minimum fluctuated values of the DC-link voltage V_{dc} of the DVR are 453 V and 426 V respectively. The settling time of the DC-link voltage is 0.41 s as shown in Fig. 5(a). Since the DC-link voltage is fluctuated seriously, the performance of the DVR to stabilize the load voltages is affected resulted in the poor compensating voltages v_{Ca}, v_{Cb}, v_{Cc} and load voltages v_{La}, v_{Lb}, v_{Lc} as shown in Figs. 5(c) and 5(d). Moreover, the transient responses of the three-phase load voltages v_{La}, v_{Lb}, v_{Lc} are still sluggish owing to the poor property of traditional PI controller. In other words, the fixed parameters of the PI controller are unsuitable for different scenarios as shown in Fig. 5(d). Furthermore, the experimental result of the DVR using FNN controller for the DC-link voltage control is represented in Fig. 6. From the experimental results, the transient responses of the DC-link voltage V_{dc} of the DVR and the three-phase load voltages v_{La}, v_{Lb}, v_{Lc} are improved at 0.4 s as shown in Figs. 6(a) and 6(d). The maximum and the minimum fluctuated values of the DC-link voltage V_{dc} of the DVR are 453 V and 437 V respectively. And the settling time of the DC-link voltage is reduced to be 0.17 s as shown in Fig. 6(a). In addition, the experimental result of the DVR using the proposed RCPFNN controller for the DC-link voltage control is provided in Fig. 7. On account of the merits of the proposed RCPFNN controller such as the online learning ability, the abilities to memorize and deal with the time-varying inputs or outputs and the capability to process the complicated spatiotemporal patterns, the transient responses of the DC-link voltage V_{dc} of the DVR and the three-phase load voltages v_{La}, v_{Lb}, v_{Lc} are much improved at 0.4 s as shown in Figs. 7(a) and 7(d). The maximum and the minimum fluctuated values of the DC-link voltage V_{dc} of the DVR are 451 V and 442 V respectively. The settling time of the DC-link voltage is much reduced

to be 0.07 s as shown in Fig. 7(a). Comparing with the experimental results as shown in Figs. 5(d), 6(d) and 7(d), the three-phase load voltages v_{La}, v_{Lb}, v_{Lc} of the DVR using the proposed RCPFNN controller can be effectively stabilized to the normal voltage level at the moment of the voltage sag. In other words, the responses of the three-phase load voltages v_{La}, v_{Lb}, v_{Lc} are smoother than the PI and FNN controllers during the sudden grid voltage sag. Additionally, to verify the online learning ability of the proposed RCPFNN controller, the waveforms of w_1^6, γ_1, m_1^2, σ_1^2, w_1^5 and t_1 of the proposed RCPFNN for the DC-link voltage control under the grid voltage sag as shown in Fig. 7 are represented in Figs. 8(a) and 8(b), respectively. From the responses shown in Fig. 8, the effectiveness of the online learning algorithm and the developed recurrent, petri properties and the compensatory operation in the proposed RCPFNN control are achieved. In other words, since the connected weights, recurrent weights, compensatory degree, mean and standard deviation of the membership functions are trained online, the proposed RCPFNN controller possesses the fast convergence capability to deal with the uncertainties for stabilizing the three-phase load voltages at the moment of the voltage sag.

The performance of the DVR under the sudden grid voltage swell is discussed. At this case, the amplitudes of the three-phase grid voltages v_{Sa}, v_{Sb}, v_{Sc} increase from its normal value by 30 % at 0.4 s. The experimental result of the DVR using PI controller for the DC-link voltage control is shown in Fig. 9. The responses of the grid voltage v_{Sa}, compensating voltage v_{Ca} of the DVR, load voltage v_{La} and the DC-link voltage V_{dc} of the DVR are provided in Fig. 9(a). The responses of the three-phase grid voltages v_{Sa}, v_{Sb}, v_{Sc} in the interval 0.38-0.48 s are illustrated in Fig. 9(b). The responses of the three-phase compensating voltages v_{Ca}, v_{Cb}, v_{Cc} of the DVR in the interval 0.38-0.48 s are represented in Fig. 9(c). The responses of the three-phase load voltages v_{La}, v_{Lb}, v_{Lc} in the interval 0.38-0.48 s are provided in Fig. 9(d). According to the experimental results, when a sudden grid voltage swell of 30 % normal value occurs at 0.4 s, the DVR can dispatch the three-phase compensating voltages v_{Ca}, v_{Cb}, v_{Cc} to stabilize the three-phase load voltages v_{La}, v_{Lb}, v_{Lc} as shown in Figs. 9(c) and 9(d). However, the transient deteriorations in the DC-link voltage V_{dc} of the DVR and the three-phase load voltages v_{La}, v_{Lb}, v_{Lc} are very serious at 0.4 s as shown in Figs. 9(a) and 9(d) on account of the poor disturbance rejection of the traditional PI controller. The maximum and the minimum fluctuated values of the DC-link voltage V_{dc} of the DVR using PI controller are 473 V and 446 V respectively. The settling time of the DC-link voltage is 0.39 s as shown in Fig. 9(a). In other words, the transient responses of the three-phase load voltages v_{La}, v_{Lb}, v_{Lc} are still sluggish and instable as shown in Fig. 9(d). Moreover, the experimental results of the DVR using the FNN and the proposed RCPFNN controllers for the DC-link voltage control under the sudden grid voltage swell are illustrated in Figs. 10 and 11, respectively. Comparing

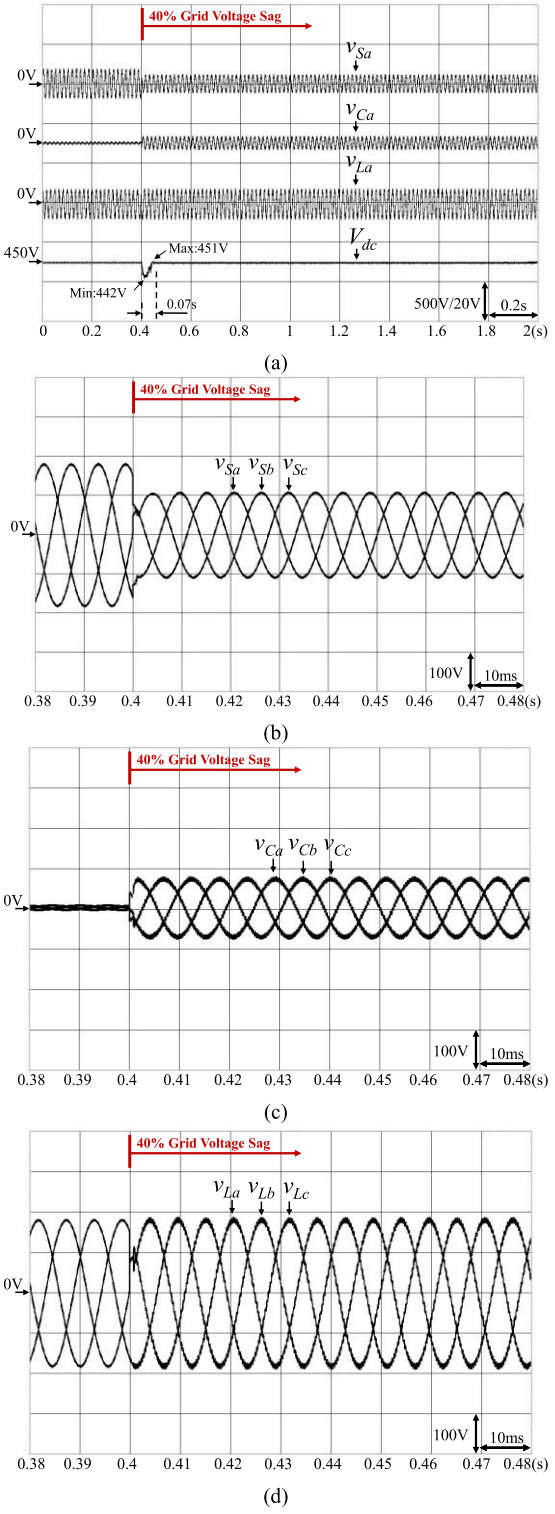

FIGURE 7. Experimental results of DVR using proposed RCPFNN controller under voltage sag. (a) Responses of grid voltage, compensating voltage of DVR, load voltage and DC-link voltage of DVR. (b) Responses of three-phase grid voltages for 0.38-0.48 s. (c) Responses of three-phase compensating voltages of DVR for 0.38-0.48 s. (d) Responses of three-phase load voltages for 0.38-0.48 s.

with the experimental results of the DVR using the PI and FNN controllers for the DC-link voltage control, the

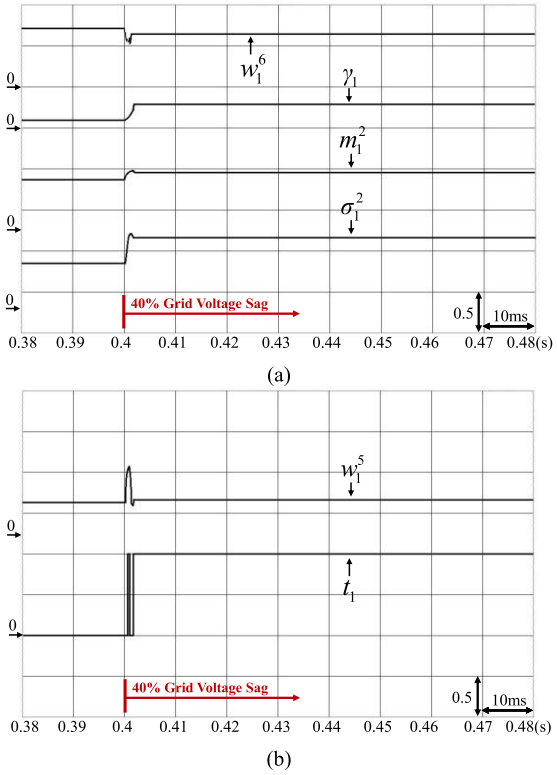

FIGURE 8. Responses of network parameters of proposed RCPFNN controller under grid voltage sag. (a) Waveforms of w_1^6, γ_1, m_1^2 and σ_1^2. (b) Waveforms of w_1^5 and t_1.

three-phase load voltages v_{La}, v_{Lb}, v_{Lc} of the DVR using the proposed RCPFNN controller can be effectively stabilized to the normal voltage level at the moment of the voltage swell as shown in Figs. 9(d), 10(d) and 11(d). The responses of the three-phase load voltages v_{La}, v_{Lb}, v_{Lc} are smoother than the PI and FNN controllers during the sudden grid voltage swell. In addition, the settling time, the overshoot to undershoot of the DC-link voltage error of the DVR using the PI, FNN and the proposed RCPFNN controllers under the grid voltage sag and swell conditions are represented in Figs. 12(a) and 12(b), respectively. According to the experimental results as shown in Figs. 5-12, the transient and steady-state responses of the three-phase load voltages v_{La}, v_{Lb}, v_{Lc} and the DC-link voltage V_{dc} of the DVR using the proposed RCPFNN controller are effectively improved and stabilized under the sudden grid voltage sag and swell conditions in consequence of the online learning ability and the powerful robust ability of the proposed RCPFNN controller.

Finally, in order to verify the feasibility and effectiveness of the DVR using the proposed RCPFNN controller for improving the transient voltage quality of the load under the sudden grid voltage unbalance, the test scenario that the amplitude of the phase-a grid voltage suddenly increases from its normal value by 30 % at 0.4 s is discussed. The experimental result of the DVR using the PI controller for the DC-link voltage control is shown in Fig. 13. The responses

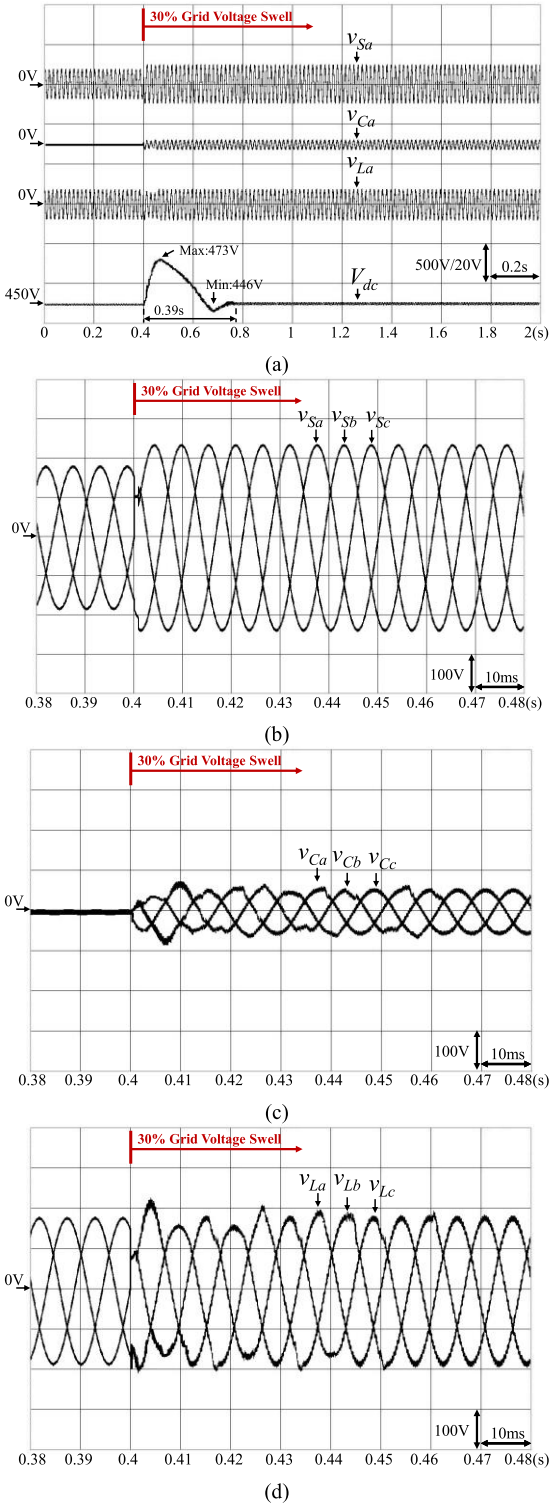

FIGURE 9. Experimental results of DVR using PI controller under voltage swell. (a) Responses of grid voltage, compensating voltage of DVR, load voltage and DC-link voltage of DVR. (b) Responses of three-phase grid voltages for 0.38-0.48 s. (c) Responses of three-phase compensating voltages of DVR for 0.38-0.48 s. (d) Responses of three-phase load voltages for 0.38-0.48 s.

of the grid voltage v_{Sa}, compensating voltage v_{Ca} of the DVR, load voltage v_{La} and the DC-link voltage V_{dc} of the

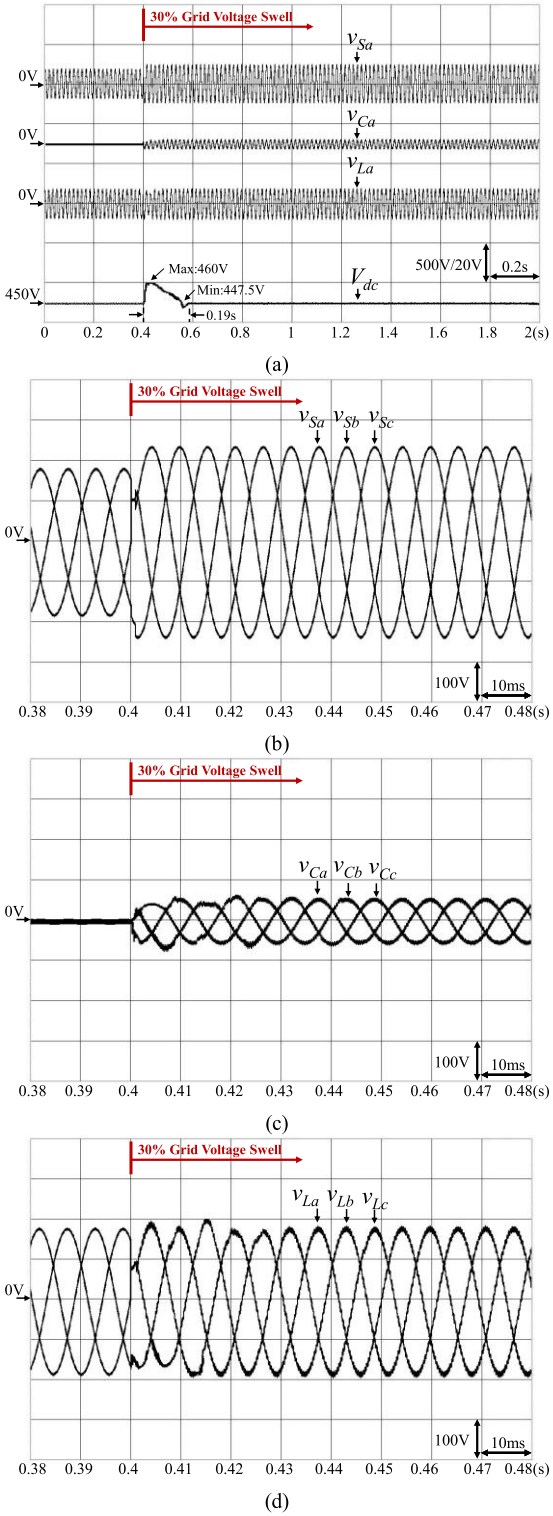

FIGURE 10. Experimental results of DVR using FNN controller under voltage swell. (a) Responses of grid voltage, compensating voltage of DVR, load voltage and DC-link voltage of DVR. (b) Responses of three-phase grid voltages for 0.38-0.48 s. (c) Responses of three-phase compensating voltages of DVR for 0.38-0.48 s. (d) Responses of three-phase load voltages for 0.38-0.48 s.

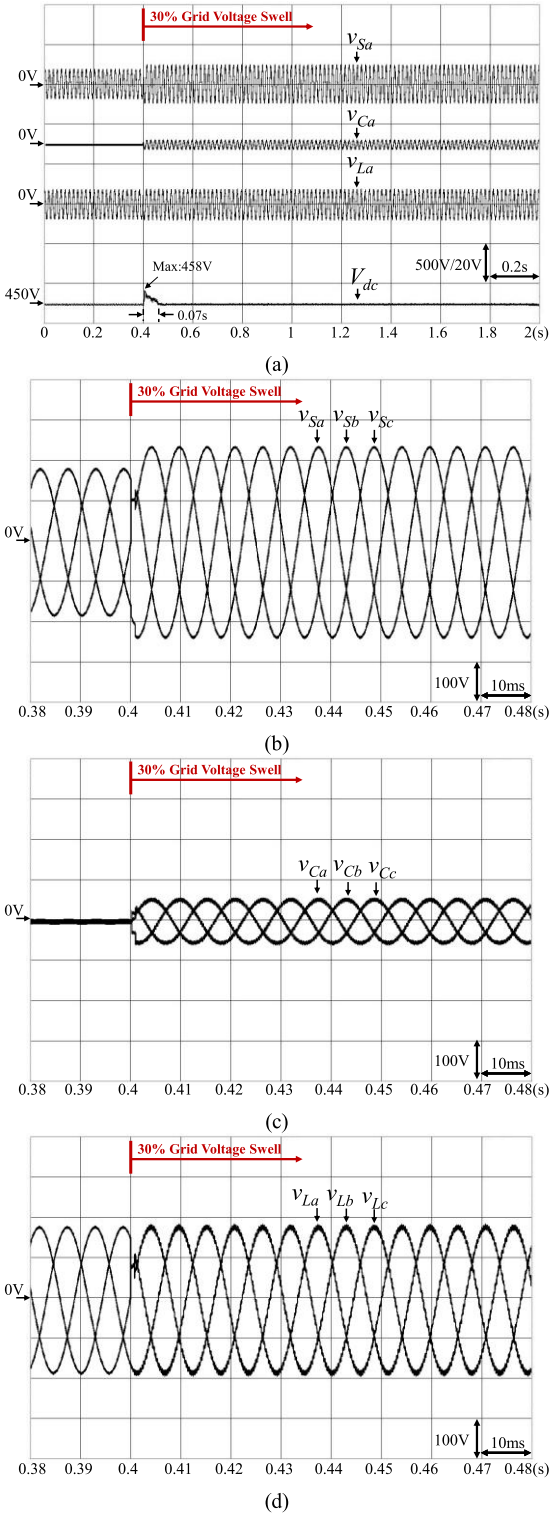

FIGURE 11. Experimental results of DVR using proposed RCPFNN controller under voltage swell. (a) Responses of grid voltage, compensating voltage of DVR, load voltage and DC-link voltage of DVR. (b) Responses of three-phase grid voltages for 0.38-0.48 s. (c) Responses of three-phase compensating voltages of DVR for 0.38-0.48 s. (d) Responses of three-phase load voltages for 0.38-0.48 s.

DVR are provided in Fig. 13(a). The responses of the three-phase unbalanced grid voltages v_{Sa}, v_{Sb}, v_{Sc} in the interval 0.38-0.48 s are given in Fig. 13(b). The responses of the three-phase compensating voltages v_{Ca}, v_{Cb}, v_{Cc} of the DVR

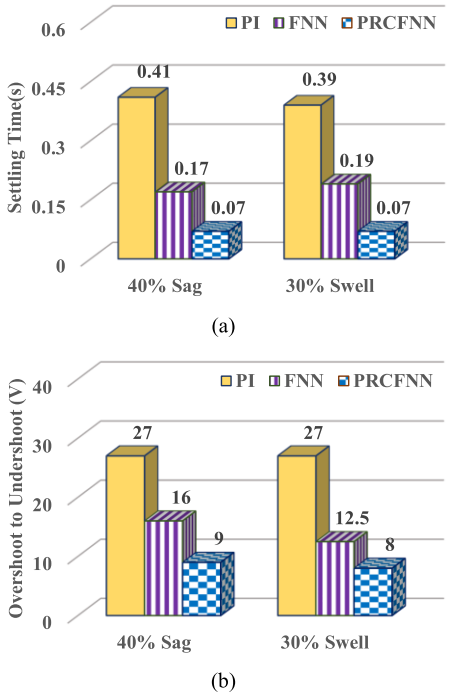

FIGURE 12. Comparison of DVR using different controllers under grid voltage sag and swell conditions. (a) Settling time of DC-link voltage. (b) Overshoot to undershoot of DC-link voltage error.

in the interval 0.38-0.48 s are provided in Fig. 13(c). The responses of the three-phase load voltages v_{La}, v_{Lb}, v_{Lc} in the interval 0.38-0.48 s are represented in Fig. 13(d). According to the experimental results, when the phase-a grid voltage suddenly increases from its normal value by 30 % at 0.4 s, the DVR can dispatch the compensating voltages v_{Ca}, v_{Cb}, v_{Cc} to stabilize the three-phase load voltages v_{La}, v_{Lb}, v_{Lc} as shown in Figs. 13(c) and 13(d). However, the maximum and the minimum fluctuated values of the DC-link voltage V_{dc} of the DVR using the PI controller are 471 V and 446 V, respectively, resulted in the transient deteriorations in the DC-link voltage V_{dc} of the DVR and the three-phase load voltages v_{La}, v_{Lb}, v_{Lc} on account of the poor disturbance rejection of the traditional PI controller as shown in Figs. 13(a) and 13(d). The settling time of the DC-link voltage is 0.36 s. Moreover, the experimental results of the DVR using the FNN and the proposed RCPFNN controllers for the DC-link voltage control under the sudden voltage unbalance are represented in Figs. 14 and 15, respectively. According to the experimental result using the proposed RCPFNN controller under the sudden voltage unbalance, the stability and the transient response of the three-phase load voltages v_{La}, v_{Lb}, v_{Lc} and the DC-link voltage V_{dc} of the DVR are better than the PI and FNN controllers at the moment of the voltage unbalance as shown in Figs. 13-15. The maximum and the minimum fluctuated values of the DC-link voltage V_{dc} of the DVR using the proposed RCPFNN controller are much reduced to be 457.5 V and 450 V, respectively. The settling time of the DC-link voltage is also much reduced to be

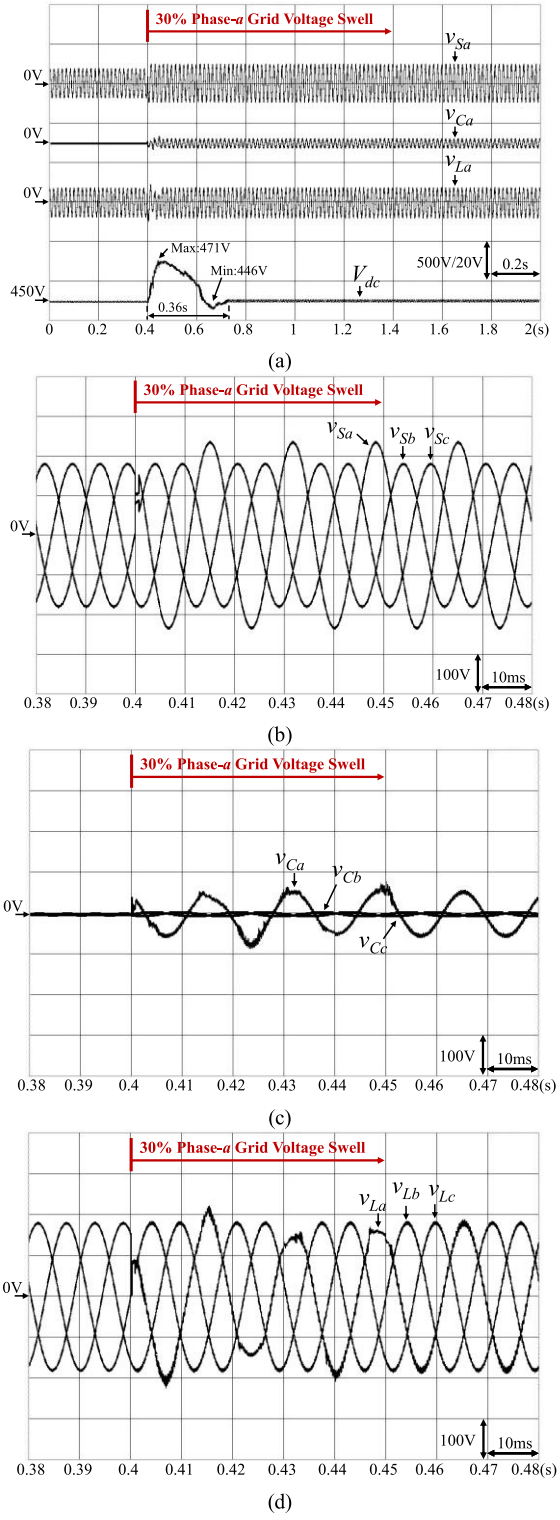

FIGURE 13. Experimental results of DVR using PI controller under voltage unbalance. (a) Responses of grid voltage, compensating voltage of DVR, load voltage and DC-link voltage of DVR. (b) Responses of three-phase unbalanced grid voltages for 0.38-0.48 s. (c) Responses of three-phase compensating voltages of DVR for 0.38-0.48 s. (d) Responses of three-phase load voltages for 0.38-0.48 s.

0.07 s as shown in Fig. 15(a). Therefore, the transient voltage quality of the load is guaranteed by using the proposed

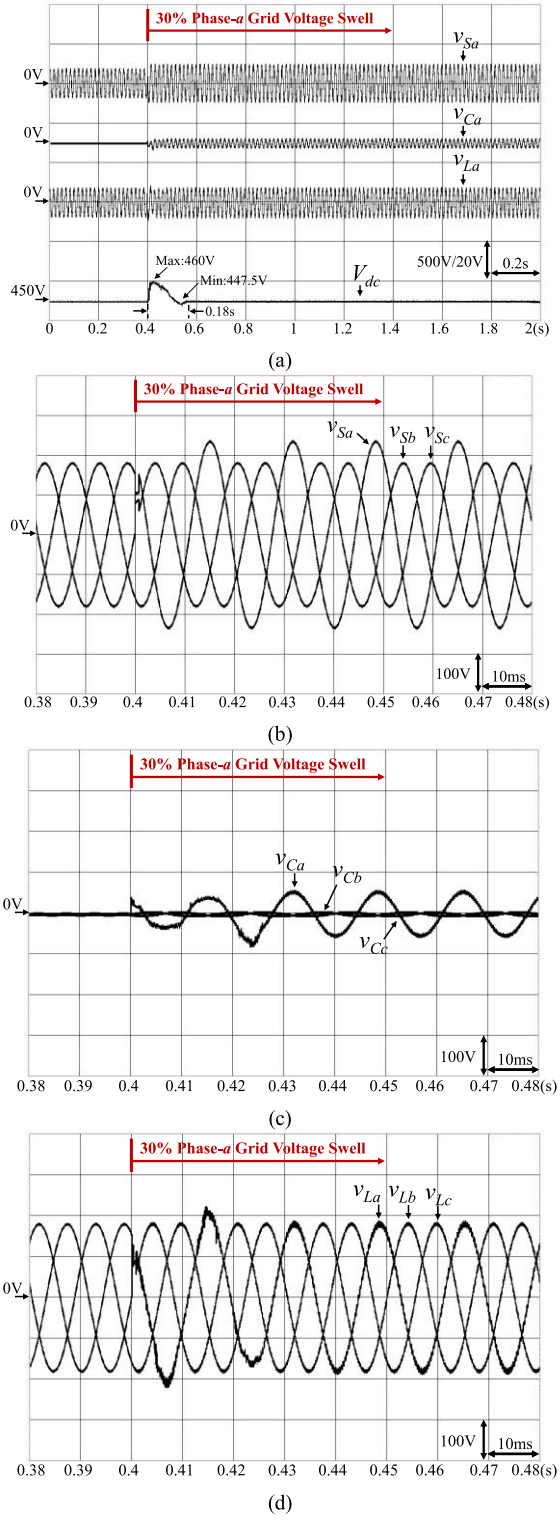

FIGURE 14. Experimental results of DVR using FNN controller under voltage unbalance. (a) Responses of grid voltage, compensating voltage of DVR, load voltage and DC-link voltage of DVR. (b) Responses of three-phase unbalanced grid voltages for 0.38-0.48 s. (c) Responses of three-phase compensating voltages of DVR for 0.38-0.48 s. (d) Responses of three-phase load voltages for 0.38-0.48 s.

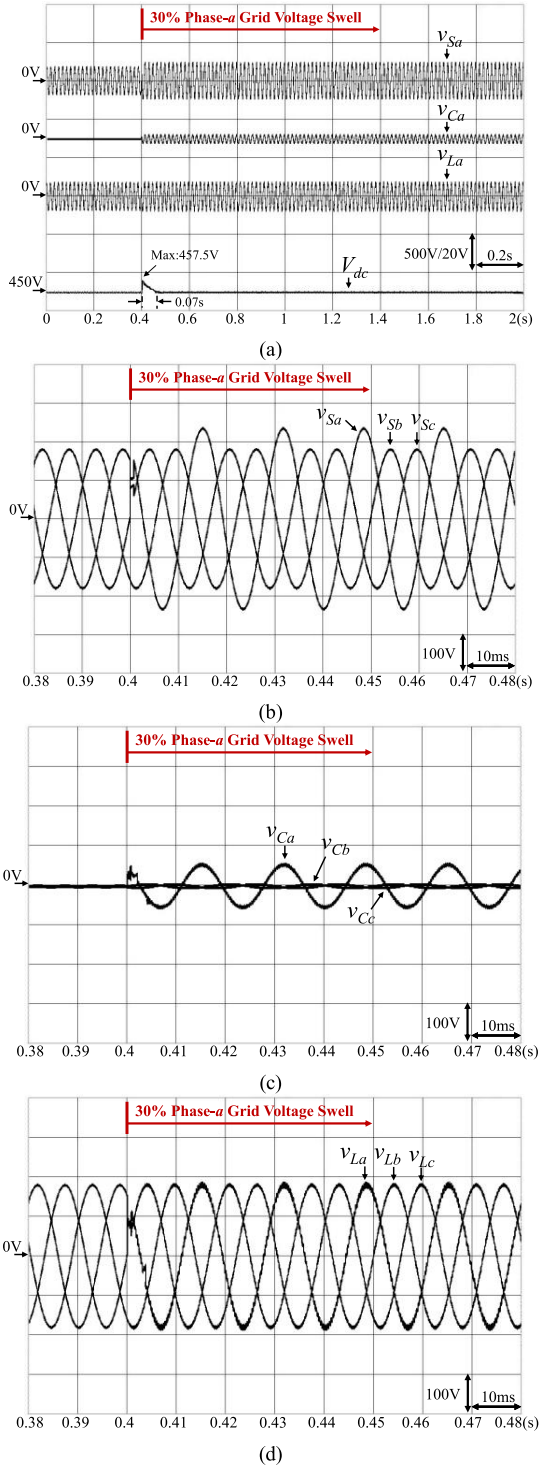

FIGURE 15. Experimental results of DVR using proposed RCPFNN controller under voltage unbalance. (a) Responses of grid voltage, compensating voltage of DVR, load voltage and DC-link voltage of DVR. (b) Responses of three-phase unbalanced grid voltages for 0.38-0.48 s. (c) Responses of three-phase compensating voltages of DVR for 0.38-0.48 s. (d) Responses of three-phase load voltages for 0.38-0.48 s.

RCPFNN controller for the DVR under the sudden grid voltage unbalance condition.

V. CONCLUSION

In this study, a DVR has been successfully developed and implemented to stabilize the three-phase load voltages

under the grid voltage sag, swell and unbalance conditions. Since the power energy follows into or out of the DC-link capacitor of the DVR resulted in the degenerate stabilization performance and the poor transient response under the sudden grid voltage distortion conditions, a novel RCPFNN controller is firstly proposed to replace the traditional PI and FNN controllers for the DC-link voltage control and the compensation strategy. Moreover, the effectiveness and the feasibility of the DVR using the proposed RCPFNN controller as the DC-link voltage controller are verified by the experimental results. According to the experimental results, owing to the online learning ability and powerful robust ability of the proposed RCPFNN controller, the transient responses of the three-phase load voltages v_{La}, v_{Lb}, v_{Lc} and the DC-link voltage V_{dc} of the DVR using the proposed RCPFNN controller are effectively improved and stabilized comparing with the PI and FNN controllers under the sudden grid voltage distortion conditions.

The major contributions of this study are: (i) the successful development of a DVR; (ii) the successful development of a novel online trained RCPFNN controller for the compensation strategy and the DC-link voltage control of the DVR; (iii) the successful implementation of the DVR using the proposed RCPFNN controller for the improvements of the three-phase load voltages and DC-link voltage under the sudden grid voltage distortion conditions, including the voltage sag, swell and unbalance.

REFERENCES

[1] E. M. Molla and C.-C. Kuo, "Voltage sag enhancement of grid connected hybrid PV-wind power system using battery and SMES based dynamic voltage restorer," *IEEE Access*, vol. 8, pp. 130003–130013, 2020.

[2] A. Benali, M. Khiat, T. Allaoui, and M. Denaï, "Power quality improvement and low voltage ride through capability in hybrid wind-PV farms grid-connected using dynamic voltage restorer," *IEEE Access*, vol. 6, pp. 68634–68648, 2018.

[3] K.-H. Tan and T.-Y. Tseng, "Seamless switching and grid reconnection of microgrid using Petri recurrent wavelet fuzzy neural network," *IEEE Trans. Power Electron.*, vol. 36, no. 10, pp. 11847–11861, Oct. 2021.

[4] F.-J. Lin, K.-H. Tan, C.-F. Chang, M.-Y. Li, and T.-Y. Tseng, "Development of intelligent controlled microgrid for power sharing and load shedding," *IEEE Trans. Power Electron.*, vol. 37, no. 7, pp. 7928–7940, Jul. 2022.

[5] S. Biricik, H. Komurcugil, N. D. Tuyen, and M. Basu, "Protection of sensitive loads using sliding mode controlled three-phase DVR with adaptive notch filter," *IEEE Trans. Ind. Electron.*, vol. 66, no. 7, pp. 5465–5475, Jul. 2019.

[6] A. Moghassemi, S. Padmanaban, V. K. Ramachandaramurthy, M. Mitolo, and M. Benbouzid, "A novel solar photovoltaic fed TransZSI-DVR for power quality improvement of grid-connected PV systems," *IEEE Access*, vol. 9, pp. 7263–7279, 2021.

[7] A. M. Gee, F. Robinson, and W. Yuan, "A superconducting magnetic energy storage-emulator/battery supported dynamic voltage restorer," *IEEE Trans. Energy Convers.*, vol. 32, no. 1, pp. 55–64, Mar. 2017.

[8] S. F. Al-Gahtani, A. B. Barnawi, H. Z. Azazi, S. M. Irshad, J. K. Bhutto, and E. Z. M. Salem, "A new technique implemented in synchronous reference frame for DVR control under severe sag and swell conditions," *IEEE Access*, vol. 10, pp. 25565–25579, 2022.

[9] P. Kanjiya, B. Singh, A. Chandra, and K. Al-Haddad, "'SRF theory revisited' to control self-supported dynamic voltage restorer (DVR) for unbalanced and nonlinear loads," *IEEE Trans. Ind. Appl.*, vol. 49, no. 5, pp. 2330–2340, Sep. 2013.

[10] P. Jayaprakash, B. Singh, D. P. Kothari, A. Chandra, and K. Al-Haddad, "Control of reduced-rating dynamic voltage restorer with a battery energy storage system," *IEEE Trans. Ind. Appl.*, vol. 50, no. 2, pp. 1295–1303, Mar. 2014.

[11] *IEEE Recommended Practice for Monitoring Electric Power Quality*, Standard IEEE 1159–2019, 1969.

[12] P. Li, L. Xie, J. Han, S. Pang, and P. Li, "New decentralized control scheme for a dynamic voltage restorer based on the elliptical trajectory compensation," *IEEE Trans. Ind. Electron.*, vol. 64, no. 8, pp. 6484–6495, Aug. 2017.

[13] A. P. Torres, P. Roncero-Sánchez, and V. F. Batlle, "A two degrees of freedom resonant control scheme for voltage-sag compensation in dynamic voltage restorers," *IEEE Trans. Power Electron.*, vol. 33, no. 6, pp. 4852–4867, Jun. 2018.

[14] P. Li, L. Xie, J. Han, S. Pang, and P. Li, "A new voltage compensation philosophy for dynamic voltage restorer to mitigate voltage sags using three-phase voltage ellipse parameters," *IEEE Trans. Power Electron.*, vol. 33, no. 2, pp. 1154–1166, Feb. 2018.

[15] M. Pradhan and M. K. Mishra, "Dual *P-Q* theory based energy-optimized dynamic voltage restorer for power quality improvement in a distribution system," *IEEE Trans. Ind. Electron.*, vol. 66, no. 4, pp. 2946–2955, Apr. 2019.

[16] P. Li, Y. Wang, M. Savaghebi, J. Lu, X. Pan, and F. Blaabjerg, "Identification design for dynamic voltage restorer to mitigate voltage sag based on the elliptical transformation," *IEEE J. Emerg. Sel. Topics Power Electron.*, vol. 9, no. 5, pp. 5672–5686, Oct. 2021.

[17] S. Kim, H.-G. Kim, and H. Cha, "Dynamic voltage restorer using switching cell structured multilevel AC–AC converter," *IEEE Trans. Power Electron.*, vol. 32, no. 11, pp. 8406–8418, Nov. 2017.

[18] J. Wang, Y. Xing, H. Wu, and T. Yang, "A novel dual-DC-port dynamic voltage restorer with reduced-rating integrated DC–DC converter for wide-range voltage sag compensation," *IEEE Trans. Power Electron.*, vol. 34, no. 8, pp. 7437–7449, Aug. 2019.

[19] A. D. Falehi and H. Torkaman, "Robust fractional-order super-twisting sliding mode control to accurately regulate lithium-battery/super-capacitor hybrid energy storage system," *Int. J. Energy Res.*, vol. 45, no. 13, pp. 18590–18612, Oct. 2021.

[20] A. D. Falehi and H. Torkaman, "Promoted supercapacitor control scheme based on robust fractional-order super-twisting sliding mode control for dynamic voltage restorer to enhance FRT and PQ capabilities of DFIG-based wind turbine," *J. Energy Storage*, vol. 42, pp. 1–23, Oct. 2021.

[21] A. D. Falehi, "Half-cascaded multilevel inverter coupled to photovoltaic power source for AC-voltage synthesizer of dynamic voltage restorer to enhance voltage quality," *Int. J. Numer. Modelling, Electron. Netw., Devices Fields*, vol. 34, no. 5, pp. 1–21, Aug. 2021.

[22] M. Osama abed elraouf, M. Aljohani, M. I. Mosaad, and T. A. AbdulFattah, "Mitigating misfire and fire-through faults in hybrid renewable energy systems utilizing dynamic voltage restorer," *Energies*, vol. 15, no. 16, pp. 1–16, Aug. 2022.

[23] Y.-Y. Lin, J.-Y. Chang, and C.-T. Lin, "A TSK-type-based self-evolving compensatory interval type-2 fuzzy neural network (TSCIT2FNN) and its applications," *IEEE Trans. Ind. Electron.*, vol. 61, no. 1, pp. 447–459, Jan. 2014.

[24] C.-J. Lin and C.-H. Chen, "Identification and prediction using recurrent compensatory neuro-fuzzy systems," *Fuzzy Sets Syst.*, vol. 150, no. 2, pp. 307–330, Mar. 2005.

[25] F.-J. Lin, K.-H. Tan, Y.-K. Lai, and W.-C. Luo, "Intelligent PV power system with unbalanced current compensation using CFNN-AMF," *IEEE Trans. Power Electron.*, vol. 34, no. 9, pp. 8588–8598, Sep. 2019.

[26] K. H. Tan, F. J. Lin, C. Y. Tsai, and Y. R. Chang, "A distribution static compensator using a CFNN-AMF controller for power quality improvement and DC-link voltage regulation," *Energies*, vol. 11, no. 8, pp. 1–17, Aug. 2018.

[27] Y.-T. Liu, Y.-Y. Lin, S.-L. Wu, C.-H. Chuang, and C.-T. Lin, "Brain dynamics in predicting driving fatigue using a recurrent self-evolving fuzzy neural network," *IEEE Trans. Neural Netw. Learn. Syst.*, vol. 27, no. 2, pp. 347–360, Feb. 2016.

[28] Y. Chu, J. Fei, and S. Hou, "Adaptive global sliding-mode control for dynamic systems using double hidden layer recurrent neural network structure," *IEEE Trans. Neural Netw. Learn. Syst.*, vol. 31, no. 4, pp. 1297–1309, Apr. 2020.

[29] K.-H. Tan, F.-J. Lin, C.-M. Shih, and C.-N. Kuo, "Intelligent control of microgrid with virtual inertia using recurrent probabilistic wavelet fuzzy neural network," *IEEE Trans. Power Electron.*, vol. 35, no. 7, pp. 7451–7464, Jul. 2020.
[30] R. J. Rodríguez, S. Bernardi, and A. Zimmermann, "An evaluation framework for comparative analysis of generalized stochastic Petri net simulation techniques," *IEEE Trans. Syst. Man, Cybern. Syst.*, vol. 50, no. 8, pp. 2834–2844, Aug. 2020.
[31] J. Li, X. Yu, and M. Zhou, "Analysis of unbounded Petri net with lean reachability trees," *IEEE Trans. Syst. Man, Cybern. Syst.*, vol. 50, no. 6, pp. 2007–2016, Jun. 2020.
[32] H. Kaid, A. Al-Ahmari, E. A. Nasr, A. Al-Shayea, A. K. Kamrani, M. A. Noman, and H. A. Mahmoud, "Petri net model based on neural network for deadlock control and fault detection and treatment in automated manufacturing systems," *IEEE Access*, vol. 8, pp. 103219–103235, 2020.
[33] F.-J. Lin, K.-C. Lu, and B.-H. Yang, "Recurrent fuzzy cerebellar model articulation neural network based power control of a single-stage three-phase grid-connected photovoltaic system during grid faults," *IEEE Trans. Ind. Electron.*, vol. 64, no. 2, pp. 1258–1268, Feb. 2017.

KUANG-HSIUNG TAN (Member, IEEE) received the B.S., M.S., and Ph.D. degrees in electrical and electronic engineering from the Chung Cheng Institute of Technology (CCIT), National Defense University, Taiwan, in 2002, 2007, and 2013, respectively. He has been a Faculty Member at CCIT, where he is currently an Associate Professor with the Department of Electrical and Electronic Engineering. His teaching and research interests include power electronics, power quality, microgrid systems, and intelligent control.

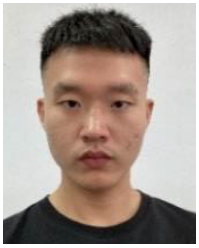

JUN-HAO CHEN received the M.S. degree in electrical engineering from National Central University, Taiwan, in 2017. He is currently pursuing the Ph.D. degree in electrical engineering with the Chung Cheng Institute of Technology (CCIT), National Defense University, Taiwan. His research interests include active power filters, intelligent control, and power electronics.

YIH-DER LEE (Member, IEEE) received the B.S. and M.S. degrees in electrical engineering from the National Taiwan University of Science and Technology, Taipei, Taiwan, in 1997 and 1999, respectively, and the Ph.D. degree in electrical engineering from National Sun Yat-Sen University (NSYSU), in 2009. From 1998 to 2010, he was an Associate Technical Specialist at Southern District Waste Management Plant, Environment Protection Bureau, Kaohsiung City Government, Taiwan. Since 2010, he has been with the Institute of Nuclear Energy Research (INER), Atomic Energy Council, and currently, he is a Researcher and the Nuclear Instrumentation Division Depute Director, which is responsible for developing microgrid and smart grid technology. His research interests include renewable energy, microgrid, power electronics, power system control, and stability.